ARTICLE

Small molecule compound M12 reduces vascular permeability in obese mice via blocking endothelial TRPV4–Nox2 interaction

Meng-ru Gao[1], Peng Zhang[2], Jing Han[2], Chun-lei Tang[1], Yi-fei Zhu[2], Hao Kan[2], Hong-juan Li[2], Xi-ping Han[1] and Xin Ma[2,1]

Transient receptor potential channel TRPV4 and nicotinamide adenine dinucleotide phosphate oxidase (Nox2) are involved in oxidative stress that increases endothelial permeability. It has been shown that obesity enhances the physical association of TRPV4 and Nox2, but the role of TRPV4–Nox2 association in obesity has not been clarified. In this study we investigated the function of TRPV4–Nox2 complex in reducing oxidative stress and regulating abnormal vascular permeability in obesity. Obesity was induced in mice by feeding a high-fat diet (HFD) for 14 weeks. The physical interaction between TRPV4 and Nox2 was measured using FRET, co-immunoprecipitation and GST pull-down assays. The functional interaction was measured by rhodamine phalloidin, CM-H_2DCFDA in vitro, the fluorescent dye dihydroethidium (DHE) staining assay, and the Evans blue permeability assay in vivo. We demonstrated that TRPV4 physically and functionally associated with Nox2, and this physical association was enhanced in aorta of obese mice. Furthermore, we showed that interrupting TRPV4–Nox2 coupling by TRPV4 knockout, or by treatment with a specific Nox2 inhibitor Nox2 dstat or a specific TRPV4 inhibitor HC067046 significantly attenuated obesity-induced ROS overproduction in aortic endothelial cells, and reversed the abnormal endothelial cytoskeletal structure. In order to discover small molecules disrupting the over-coupling of TPRV4 and Nox2 in obesity, we performed molecular docking analysis and found that compound M12 modulated TRPV4–Nox2 association, reduced ROS production, and finally reversed disruption of the vascular barrier in obesity. Together, this study, for the first time, provides evidence for the TRPV4 physically interacting with Nox2. TRPV4–Nox2 complex is a potential drug target in improving oxidative stress and disruption of the vascular barrier in obesity. Compound M12 targeting TRPV4–Nox2 complex can improve vascular barrier function in obesity.

Keywords: obesity; TPRV4; Nox2; oxidant stress; vascular permeability; Compound M12

INTRODUCTION

The vascular endothelium plays an important role in regulating the exchange of substances. Impairment of endothelial permeability and barrier function can lead to a variety of diseases such as thrombosis and atherosclerosis [1]. ROS plays a vital role in regulating endothelial permeability [2]. Also, obesity triggers a state of low persistent inflammation, which causes oxidative stress in different tissues [3]. Understanding the mechanism of ROS generation in obesity is therefore crucial to prevent cardiovascular diseases.

TRPV4 is a cation channel that is found in many parts of the body, such as the heart and blood vessels [4]. Recent studies have shown that the use of agonists to activate TRPV4 increases the generation of ROS by causing calcium ions to flow into endothelial cells (ECs) [5–7].

Nox2 (nicotinamide adenine dinucleotide phosphate oxidase), a member of the NADPH oxidase family, was originally identified in neutrophils and can regulate the production of ROS. Recent studies have revealed that Nox2 is expressed in cardiomyocytes and ECs, in addition to leukocytes and many non-hematopoietic

cells, and functions as a pathway regulating redox-sensitive signaling [8].

Both TRPV4 and Nox2 play a role in the regulation of oxidative stress, and recent studies have shown that they form complexes to function [9, 10]. However, their effect in mediating obesity-induced oxidative stress is unclear. Therefore, we conducted this study to investigate the role of the TRPV4–Nox2 complex.

MATERIALS AND METHODS

Mice

In this study, the wild-type (WT) C57BL/6J mice we used were 4–8 weeks old and were obtained from the Model Animal Resource Information Platform (Nanjing, China). The TRPV4-knockout (TRPV4 KO) [11] mice on the C57BL/6J background were donated by Dr. Makoto Suzuki (Jichi Medical School, Tochigi, Japan and RIKEN BioResource Center, Japan). All mice were maintained in accordance with the prescribed conditions (22 ℃, 12 h day/night cycle, air-filtered, and pathogen-free conditions), and TRPV4 KO and WT C57BL/6J mice littermates were identified by PCR assay

(Supplementary Fig. S1). To make diet-induced obese mice, we selected 4-week-old WT C57BL/6J mice fed a high-fat diet (HFD) in which 45% of calories were derived from fat. Control mice were fed a normal diet (ND) with 25% of calories as fat. After 14 weeks, the body weight, blood glucose and TG, LDL would increase in HFD mice and TG, HDL would decrease (Supplementary Fig. S2), which showed that the mouse model was successful [12]. All experimental protocols used in this study were reviewed and approved by the Animal Experimentation Ethics Committee of Jiangnan University (approval number: JN. No 20200515c0501230[061]), and all operations were in strict accordance with the Guide for the Care and Use of Laboratory Animals (National Institutes of Health publication, 8th edition, updated 2011).

Cell preparation and culture

Primary aortic ECs were isolated from ND, HFD mice, TRPV4-KO mice fed with a normal diet (TRPV4 KO-ND), and TRPV4-KO mice fed with a high-fat diet (TRPV4 KO-HFD). Briefly, after euthanasia using CO_2, the thorax was opened, and the aorta was quickly dissected out and placed in cold sterile phosphate-buffered saline (PBS). After washing with PBS, the aorta was minced and digested with 0.2% collagenase (C9891, Sigma-Aldrich, Darmstadt, Germany) in PBS for 25 min at 37 °C. After digestion, the cells were centrifuged at $845 \times g$ for 5 min and the pelleted cells were resuspended in ECM complete medium (1001, ScienCell, San Diego, California, U.S.A) and incubated in six-well cell culture plates for 2 h, after which they were washed with PBS to remove non-adherent cells. The ECs were cultured in ECM for 1–2 d and then used for experiments [13]. The identification of ECs was performed using flow cytometry. As can been seen in Supplementary Fig. S3, the ECs we isolated were able to be labeled with CD31 (anti-mouse, ab9498, Abcam, Shanghai, China, 1:200). HEK-293 cells (CRL-1573, ATCC, Manassas, Virginia, U.S.A.) were purchased from ATCC.

Immunofluorescence analysis and FRET

Briefly, the tissue samples were washed with PBS and incubated in PBS containing 5% bovine serum albumin (BSA) and 1% Triton X-100 for 30 min. Then they were incubated with the primary antibodies rabbit polyclonal anti-TRPV4 (anti-rabbit, ACC-034, Alomone Laboratories, Jerusalem, Israel) and Nox2 monoclonal anti-Nox2 (anti-mouse, sc-130543, Santa-Cruz Biotech, Dallas, Texas, U.S.A) overnight at 4 °C under humidified conditions. Thereafter, the samples were washed and incubated with secondary antibodies (Alexa Fluor 488/568, Invitrogen, Carlsbad, California, U.S.A, 1:200) at room temperature. After 1 h incubation, the samples were washed and mounted. The fluorescence images were acquired and the FRET efficiency was measured using a confocal microscope (Leica TCS SP8, Wetzlar, Germany) [14].

Co-immunoprecipitation

Briefly, ECs were isolated, grown to 90% confluence, harvested, and lysed in lysis buffer. The lysate was centrifuged at $11,000 \times g$ for 10 min, then the supernatant was removed and incubated with protein A + G agarose beads (sc-2003, Santa-Cruz Biotech, Dallas, Texas, U.S.A) at 4 °C for 30 min to remove nonspecific binding. The protein sample concentrations were adjusted to be consistent across groups. Then the indicated antibodies were added to the protein samples and incubated at 4 °C overnight. After incubation, 50 μL of protein A + G agarose beads was added to the mixture and incubated at 4 °C for 4 h. The mixture was centrifuged at $400 \times g$ for 5 min, then the beads were removed and washed 6 times with PBS. Then, 20 μL of SDS sample buffer was added to the beads and boiled for 5 min to elute the precipitated proteins, which were then analyzed using Western blotting.

Western blotting

In this experiment, protein samples were separated using 10% SDS-PAGE SDS-Tris glycine gel electrophoresis. After separation,

the samples were transferred to a PVDF membrane and blocked using Tris-buffered saline (TBS) buffer containing 0.1% Tween-20 (TBST) and 5% nonfat dry milk for 2 h. After this step, primary antibodies were added to the membranes and kept at 4 °C overnight. The following antibodies were used: anti-Nox2 (anti-mouse, sc-130543, Santa-Cruz Biotech, Dallas, Texas, U.S.A, 1:200), anti-Nox2 (anti-rabbit, ab129068, Abcam, Shanghai, China, 1:200), and anti-TRPV4 (anti-rabbit, ACC-034, Alomone Laboratories, Jerusalem, Israel, 1:200). Next, horse-radish peroxidase-conjugated secondary antibody (A16072SAM-PLE, A16104SAMPLE, Invitrogen, Carlsbad, California, U.S.A, 1:200; 58802S, Cell Signaling, Beverly, MA, U.S.A, 1:200) was added and incubated for 2 h. After the above steps, the blots were washed using TBST. Then the blots were developed with ECL substrate (P0018, Beyotime Biotechnology, Shanghai, China) and imaged with the ChemiDoc XRS+ System (Bio-Rad, Hercules, California, U.S.A.).

Rhodamine phalloidin staining assay

The cell samples were fixed in 4% PFA, permeabilized with 0.1% Triton X-100 for 10 min, and blocked with 5% BSA for 1 h. Rhodamine phalloidin (R415, Invitrogen, Carlsbad, California, U.S.A) was dissolved in methanol at 6.6 μM and stored at −20 °C. Just prior to use, phalloidin was diluted (1:40) in 1% BSA. The samples were incubated with diluted phalloidin[15] for 30 min. Nuclei were stained with DAPI (1:1000 in PBS) by incubation for 10 min. Then, the samples were washed three times with PBS for 5 min each. Images of F-actin were captured on a confocal microscope (Carl Zeiss LSM880, Oberkochen, Germany).

Analysis of ROS and superoxide generation

The intracellular generation of ROS was measured by CM-H_2DCFDA (Molecular Probes, C6827, Invitrogen, Carlsbad, California, U.S.A.) [16]. Briefly, primary aortic cells (1×10^5) were seeded in 35-mm laser confocal Petri dishes. After 12 h, the cells were washed with normal saline buffer solution (NPSS) to remove the residual medium. The cells were incubated with CM-H_2DCFDA for 15 min at 37 °C in a humidified, dark environment. Then the cells were washed again with NPSS, and images were captured by a fluorescence microscope (Carl Zeiss LSM880, Oberkochen, Germany). The relative CM-H_2DCFDA fluorescence was calculated as follows. In each sample, three areas were randomly selected for imaging, the fluorescence intensity (minus the background fluorescence) of each image was measured, and the average of three values was calculated to give the relative fluorescence intensity.

DHE staining

To assess the level of oxidative stress, freshly isolated aortic tissue was incubated with 2 μM DHE (S0063, P0018, Beyotime Biotechnology, Shanghai, China) for 60 min at 37 °C in the dark [17]. Then, the tissue was washed three times with PBS and the fluorescence was measured with the confocal microscope (Carl Zeiss LSM880, Oberkochen, Germany).

In vitro permeability assay

In brief, primary aortic ECs were isolated and cultured in six-well cell culture plates. After the cells reached 80% confluence, they were digested and seeded into Transwell chambers; 500 μL of ECM complete medium was added to the upper chamber and 1500 μL of ECM complete medium to the lower chamber. After the cells formed a monolayer, they were washed with PBS, and 100 μL, 5 μM fluorescein isothiocyanate (FITC)-dextran (sc-263323, Santa-Cruz Biotech, Dallas, Texas, U.S.A.) was added to the upper chamber and 600 μL of PBS to the lower chamber. The cells were incubated for 1 h, then the fluorescence intensity of the PBS (100 μL) in the lower chamber was measured

(Synergy H4, Winooski, Vermont, U.S.A) at excitation wavelength of 494 nm and emission wavelength of 521 nm.

Evans Blue permeability assay

Mice were anesthetized with intraperitoneal sodium pentobarbital (60 mg/kg). Evans Blue dye (5 mg/kg, 1%; Sigma-Aldrich, Darmstadt, Germany) was injected into the inferior vena cava to stain the aorta via the systemic circulation. After incubation for 30 min, the mice were euthanized with CO_2. The aorta was quickly removed and photographed under a light microscope. To quantify the aortic permeability, free Evans Blue was removed by PBS perfusion. Then the aorta was weighed and cut into pieces. The Evans Blue in tissue was extracted with 5% PFA overnight at 55 °C, its concentration was measured on a spectrophotometer at 620 nm, and the content per gram of tissue was calculated.

Molecular docking and plasmid mutations

The potential binding sites between TRPV4 and Nox2 were found using BIOVIA Discovery Studio 2018 software. The protein crystal structures were downloaded from the PDB website. TRPV4: PDB accession number 4DX1; Nox2: PDB accession number 3A1F.

With this software, we found ten binding sites and then carried out mutagenesis on them [18]. All the primers we used were shown in Supplementary Table 1. The ten amino-acid sequences were as follows:

TRPV4		Nox2	
△AR1 (aa 261–267)	GADVHAQ	△1 (aa 1–9)	IAVDGPFGT
△AR2 (aa 305–312)	TENPHKKA	△2 (aa 10–18)	ASEDVFSYE
△AR3 (aa 313–321)	DMRRQDSRG	△3 (aa 60–68)	LCRDTHAFE
△AR4 (aa 352–361)	KCARLFPDSN	△4 (aa 145–152)	NTTIGVFL
△AR5 (aa 362–371)	LEAVLNNDGL	△5 (aa 152–160)	LCGPEALAE

Construction of endothelial cell-specific adeno-associated viruses

To produce endothelial cell-specific AAVs, we first prepared pAOV.SYN.3FLAG plasmids. By sub-cloning assays, we then sub-cloned the Nox2 and Nox2 mut genes into pAOV.SYN.3FLAG to produce the desired plasmid carrying the target gene fragment. This plasmid had Flt1, an endothelial cell-specific promoter, and mScarlet, a red fluorescent protein gene. After these steps, the AAV-Flt-Nox2 and AAV-Flt1-Nox2 mut were produced by transfection of AAV-293 cells with these constructed plasmids, along with AAV helper plasmid (pAAV Helper) and AAV Rep/Cap expression plasmid. The viruses were purified by iodixanol step-gradient ultracentrifugation to provide endothelial cell-specific adeno-associated viruses (AAV) for this study.

Statistical analyses

In each experiment, the ECs and mice in the different treatment groups were randomly divided. All statistical analyses were done with GraphPad Prism 8.0 software. All data are expressed as the mean ± SEM. Comparisons between two sets of data that conformed to normality and had equal variance used Student's t test followed by the unpaired two-tailed t test; otherwise, appropriate nonparametric tests were used (Student's t test followed by the Mann–Whitney test). Data from more than two groups were analyzed using analysis of variance (ANOVA) test followed by Tukey's multiple comparison test if they met normality and had equal variances; otherwise, appropriate nonparametric tests were used (one-way ANOVA test followed by Dunnett's multiple comparison test). We considered $P < 0.05$ to represent a significant difference between results.

RESULTS

Physical interaction of TRPV4 and Nox2 is enhanced in obesity

To investigate the physical interaction between the two proteins, TRPV4 and Nox2, in obesity, we first performed co-immunoprecipitation assays using aortic ECs. We found that the anti-TRPV4 antibody could pull-down Nox2 in the protein lysates freshly prepared from ND and HFD aortic ECs (Fig. 1a). However, compared to the level of Nox2 pulled down from ND aortic ECs, more Nox2 could be detected in the HFD group, suggesting that the physical association between TRPV4 and Nox2 is stronger in HFD mice than in mice on a ND (Fig. 1a). Of course, we also detected the association between TRPV4 and other Noxs before. Although there was a physical association between TRPV4 and Nox1 or Nox4, the association of other Noxs with TRPV4 was significantly lower than Nox2 (Supplementary Fig. S4). Next, to further confirm the effect of obesity on physical association between these two proteins, we carried out immuno-FRET assays. As shown in Fig. 1b, c, a stronger FRET signal was detected in arterial segments isolated from HFD mice (Fig. 1b, c), indicating that the physical association of TRPV4–Nox2 was increased in the arterial segments from HFD mice. Then, to explore whether this association of TRPV4–Nox2 was direct, we performed GST pull-down assay. The results showed that GST-TRPV4 could efficiently pull-down His-Nox2 (Fig. 1d), strongly indicating that TRPV4 directly interacted with Nox2 in vitro.

TRPV4 and Nox2 are involved in the regulation of ROS production and cell permeability in obesity

Next, before exploring whether there is also a functional codependence between TRPV4 and Nox2, we first examined the role of TRPV4 and Nox2 in obesity. Firstly, we used CM-H_2DCFDA staining assays to measure the level of ROS, based on previous studies [19, 20]. As shown in Fig. 2, there was almost no difference in the basal ROS levels between ND and TRPV4 KO-ND group. While, after treatment with 100 nM GSK1016790A (a specific TRPV4 agonist), a significant rise (~65%) in ROS levels was observed in ND aortic ECs (Fig. 2a). In aortic ECs isolated from TRPV4 KO-ND mice, although there was a ~21% increase in GSK-induced ROS production compared to TRPV4 KO-ND group, the increase was significantly reduced compared to the ND + GSK group (Fig. 2a). These data indicates that TRPV4 is involved in regulating ROS production. Then, as shown in Fig. 2b, the generation of ROS was increased in the HFD group (Fig. 2b). Nox2 dstat (a specific Nox2 inhibitor) [21–23], HC067046 (a specific TRPV4 inhibitor) and TRPV4-KO inhibited this increase (Fig. 2b and Supplementary Fig. S5a), confirming the involvement of TRPV4 and Nox2 in the regulation of obesity-induced ROS overproduction.

Obesity causes many diseases, one of which is altered vascular permeability [24, 25]. VE-cadherin is known to control intercellular junctions [26–28], its downregulation decreases endothelial barrier function [29, 30]. ICAM-1, the most extensively studied intercellular adhesion molecule, is activated and up-regulated by ROS [31]. Furthermore, previous studies have shown that overexpression of ICAM-1 is one of the causes of increased EC permeability [32–34]. So first, we assessed the levels of VE-cadherin and ICAM-1 mRNA expression in mouse aortic ECs. The results showed that the mRNA level of VE-cadherin expression was decreased and ICAM-1 was increased in the HFD group (Fig. 2c, d). While the expression of both mRNA was reversed in TRPV4-KO group and HFD aortic ECs pretreated with Nox2 dstat (Fig. 2c, d) and HC067047 (Supplementary Fig. S5b) group. These results suggest that the changes induced by obesity in VE-cadherin and ICAM-1 expression are regulated by TRPV4 and Nox2. We used rhodamine phalloidin staining assays to visualize cell F-Actin, another assessment of cell permeability. Through these data, we found that obesity-induced a significant rearrangement of the endothelial cytoskeletal structure, while this change was reversed in the TRPV4 KO, Nox2 dstat (Fig. 2e) and
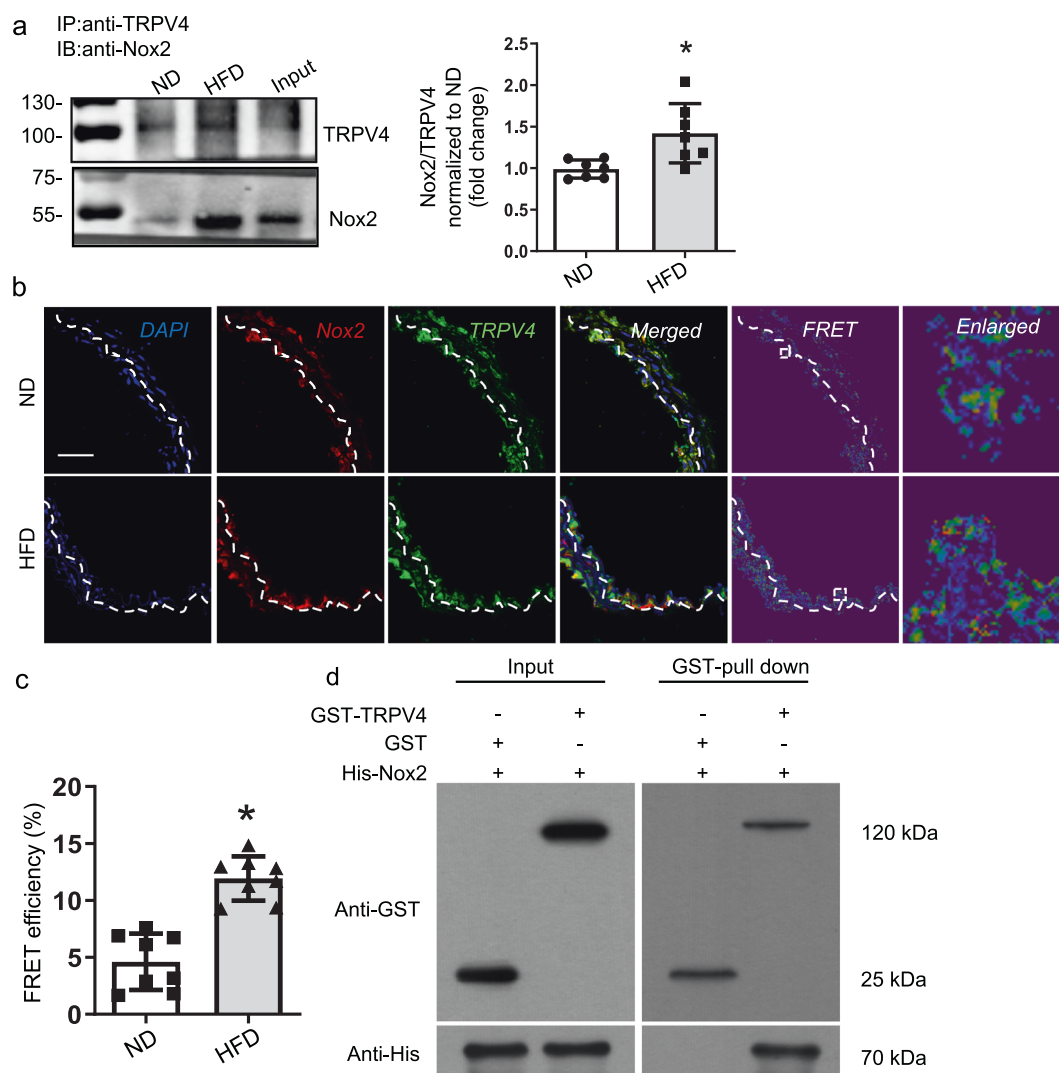
Fig. 1 The physical association between TRPV4 and Nox2 is enhanced in obesity. a Left, co-Immunoprecipitation of TRPV4 and Nox2 in primary aorta endothelial cells; right, band intensities normalized to TRPV4 ($n = 7$ mice; *$P = 0.0070$ vs. ND; Student's t test and Mann–Whitney test; ND, Wild-type C57BL/6J mice fed with normal diet; HFD, Wild-type C57BL/6J mice fed with high-fat diet). **b** Representative fluorescence resonance energy transfer (FRET) images of aorta sections from ND and HFD mice (dashed white lines, autofluorescence of elastin; scale bar, 100 μm); (**c**) Quantification of FRET efficiency of aorta sections from ND ($n = 9$) and HFD ($n = 9$) mice (*$P = 0.0025$ vs. ND, Student's t test, unpaired two-tailed t test). **d** Direct interaction between TRPV4 and Nox2 was demonstrated by in vitro GST pull-down assay. All data are shown as the mean ± SEM.

HC067047 (Supplementary Fig. S5c) group. Using FITC-dextran for in vitro permeability experiments [35, 36], we found that its extravasation was also significantly increased in obesity (2-fold increase compared to ND group (Fig. 2f)). However, in TRPV4 KO and Nox2 dstat, the exudation of dye decreased to about 68% (TRPV4-KO group) and 71% (Nox2 dstat group) compared to HFD group (Fig. 2f). Besides, as shown in Supplementary Fig. S5d, obesity-induced increase in exudation of dye was inhibited by HC067047 (Supplementary Fig. S5d). These results showed that obesity-induced cell permeability increase is regulated by TRPV4 and Nox2.

TRPV4 is important for the regulation of vascular permeability in obesity
Next, to further investigate the functional role of these proteins in regulating ROS production and vascular permeability, a DIO mouse model was used to do these assays again. DHE staining assays showed that the ROS fluorescence intensity was highly elevated in HFD arterial segments (Fig. 3b). Rhodamine phalloidin staining assays demonstrated that obesity induced a significant

rearrangement of cytoskeletal structure (Fig. 3a). Then, as described in previous studies, Evans Blue staining is the gold standard to test vascular permeability [37, 38]. Previous studies showed that Evans Blue can be used for testing aorta permeability [39, 40]. So we next used Evans Blue staining assays to assess the vascular permeability of mouse aorta. Consistently, obesity triggered a remarkable increase in the exudation of Evans Blue dye (Fig. 3c). However, there were no significant changes in TRPV4-KO mice fed with normal diet (TRPV4 KO-ND) or TRPV4-KO mice fed with high-diet (TRPV4 KO-HFD) (Fig. 3c). These results further emphasize the importance of TRPV4 in regulating excessive oxidative stress and vascular barrier disruption in obesity.

TRPV4-ΔAR4 and Nox2-Δ4 account for the association between TRPV4 and Nox2
Next, to explore the role of TRPV4–Nox2 association in the regulation of ROS production and vascular permeability and determine whether there is also a functional association between TRPV4 and Nox2, we conducted the following experiments. First,
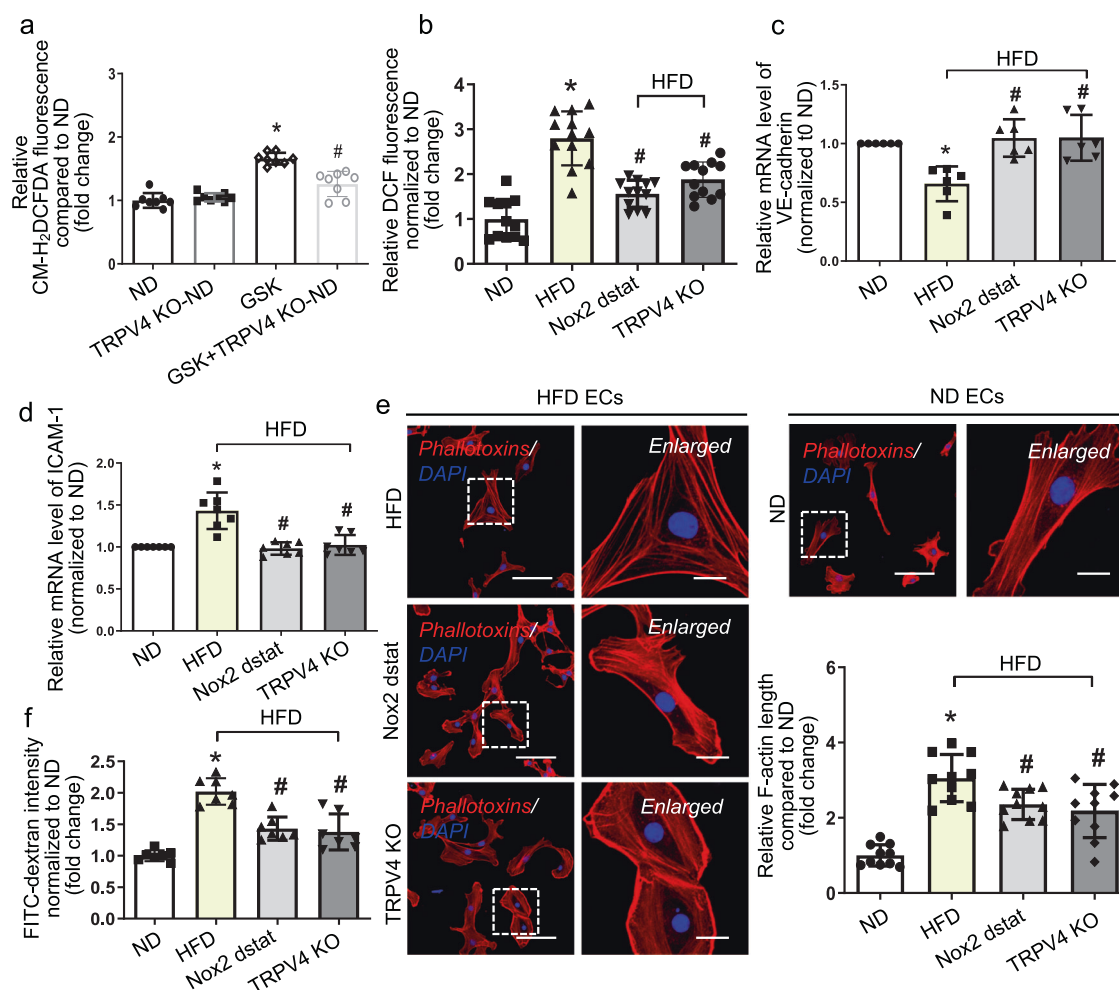
Fig. 2 Functional role of TRPV4 and Nox2 in ECs in obesity. a 5,6-Chloromethyl-2′,7′-dichlorodihydrofluorescein diacetate (CM-H₂DCFDA) staining results showing the GSK (100 nM)-induced reactive oxygen species (ROS) in ND aortic ECs and TRPV4-KO aortic ECs ($n = 8$, $^*P < 0.05$ vs. Ctrl, $^\#P < 0.05$ vs. GSK, one-way ANOVA, Dunnett's multiple comparisons test). **b** Statistics of CM-H₂DCFDA fluorescence intensity in mouse aortic ECs isolated from ND mice, HFD mice with or without Nox2 dstat and TRPV4-KO mice ($n = 12$, $^*P < 0.05$ vs. ND, $^\#P < 0.05$ vs. HFD, one-way ANOVA, Tukey's multiple comparisons test). **c, d** Relative mRNA level of VE-cadherin and ICAM-1 in ND, HFD, TRPV4-KO aortic ECs and HFD aortic ECs pretreated with Nox2 dstat ($n = 6$; $^*P < 0.05$ vs. ND, $^\#P < 0.05$ vs. HFD, Student's t test, Paired t test). **e** Representative photomicrographs of rhodamine phalloidin staining and statistical results of F-actin length (scale bars, 100 μm), normalized to ND, ($n = 10$ mice; $^\#P < 0.05$ vs. HFD, $^*P < 0.05$ vs. ND; one-way ANOVA, Tukey's multiple comparisons test). **f** Results of FITC-dextran staining assays showing permeability of ND, HFD, TRPV4-KO aortic ECs and HFD aortic ECs pretreated with Nox2 dstat ($n = 8$ mice; $^*P < 0.05$ vs. ND, $^\#P < 0.05$ vs. HFD, one-way ANOVA, Tukey's multiple comparisons test). All data are shown as the mean ± SEM.

in vitro experiments were performed. Using molecular docking techniques, we found a series of binding domains of the TRPV4–Nox2 complex. We then mutated these domains and performed FRET assays in human embryonic kidney (HEK) cells co-expressing TRPV4 and Nox2 to confirm the function of these domains in regulating TRPV4–Nox2 interactions. The results showed that deletion of the region TRPV4-ΔAR4 (aa 352–361) and the region Nox2-Δ4 (aa 145–152) significantly decreased the FRET signal of TRPV4 and Nox2 (Fig. 4a). These results suggest that TRPV4-ΔAR4 and Nox2-Δ4 account for the association between TRPV4 and Nox2 (Fig. 4a). Next, to further detect whether the deleted 8 amino acids on Nox2 are indeed essential for the binding, we performed GST pull-down assay. The results showed that GST-TRPV4 could efficiently pull-down His-Nox2 but not His-Nox2-Δ4, indicating that the mutation of Nox2 could destroy this interaction (Fig. 4c).

Disrupting the TRPV4–Nox2 association reduces vascular permeability
After these experiments, we then generated an AAV vector that expressed Nox2 (AAV-Flt1-Nox2) and Nox2-Δ4 (AAV-Flt1-Nox2

mut) (OBiO Technology, Shanghai, China). Intravenously injected AAV effectively infected the endothelium (Supplementary Fig. S6) and altered the physical association of TRPV4–Nox2 in aortic ECs (Fig. 4b). Using these viruses for the next experiments, we found that overexpression of Nox2-Δ4 in the HFD mice by intravenously injected AAV-Flt1-Nox2 mut significantly reduces the fluorescence intensity of CM-H₂DCFDA (Fig. 5a) and DHE (Supplementary Fig. S7a), which suggested that overexpression of Nox2-Δ4 helps reduce ROS production. Then using rhodamine phalloidin and FITC-dextran staining assay to detect the change in permeability, we could see that after overexpressing of Nox2 Δ4, cytoskeletal rearrangement was significantly reversed and the degree of FITC-dextran extravasation was remarkably decreased (to ~72% compared to HFD) (Fig. 5b, d). These results suggest that the increased aortic ECs permeability is effectively improved by Nox2 Δ4 overexpression. Using Evans Blue staining assay to observe the aorta permeability, the same results were achieved. The AAV-Flt1 Nox2 mut induced a significant decrease in the exudation of Evans Blue dye, indicating that overexpression of Nox2-Δ4 can help prevent the increased permeability in HFD aorta (Fig. 5e). Then, at
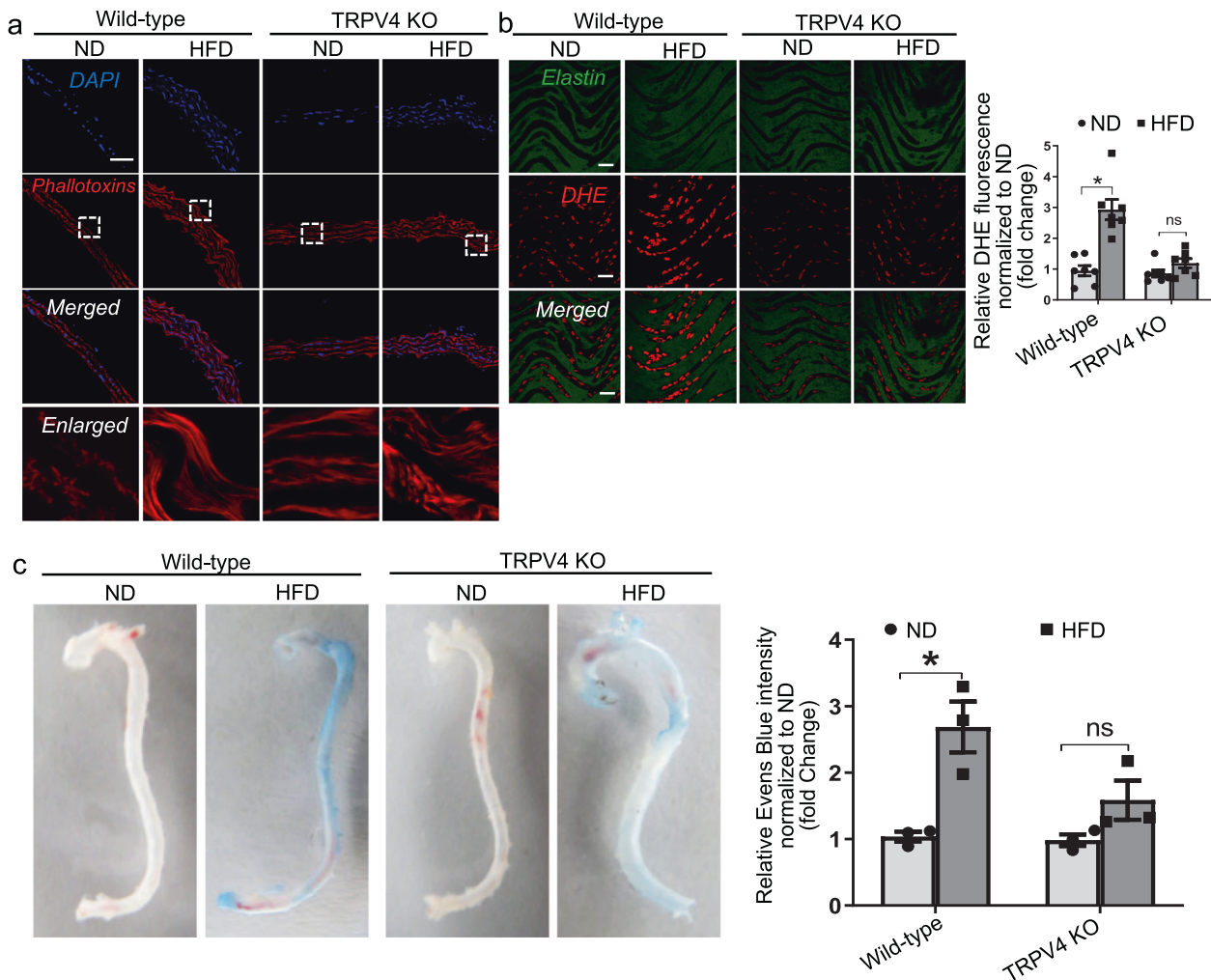
Fig. 3 TRPV4 is involved in the regulation of ROS production and vascular permeability in diet-induced obesity mouse model. **a** Representative photomicrographs of rhodamine phalloidin staining in arterial sections from ND, HFD, TRPV4 KO-ND, TRPV4 KO-HFD mice (scale bar, 50 μm). **b** Right, representative photomicrographs of dihydroethidium (DHE) staining in arterial sections from ND, HFD, TRPV4 KO-ND, TRPV4 KO-HFD mice; left, analysis of DHE fluorescence intensity normalized to the value in control aorta ($n = 6$–7 mice; wild-type, *$P = 0.0022$ vs. ND, TRPV4-KO, $P = 0.1189$ vs. ND, Student's t test, Mann–Whitney test; scale bars, 50 μm). **c** Aortic permeability under normal and high-fat conditions in wild-type and TRPV4-KO mice. Relative content of Evans blue per gram aorta normalized to control aorta ($n = 3$ mice; wild-type, *$P = 0.0132$ vs. ND; TRPV4-KO, $P = 0.1210$ vs. ND, Student's t test, unpaired two-tailed t test). All data are shown as the mean ± SEM.

the mRNA level, we could see that the changes in VE-vadherin and ICAM-1 expression were consistent with these results (Fig. 5c). Overexpression of Nox2 Δ4 increased VE-cadherin and decreased ICAM-1 mRNA expression in HFD aortic ECs (Fig. 5c). However, these changes were absent in TRPV4-KO mice fed with high-fat diet (TRPV4 KO-HFD) (Fig. 5f–j and Supplementary Fig. S7b). These data demonstrate that overexpression of Nox2 Δ4 can help reduce ROS production and vascular permeability in obesity. Besides, the mutation of Nox2 did not affect its expression and function (Supplementary Fig. S8), but only decreased its association with TRPV4 (Fig. 4b). These prompted us to believe AAV-Flt1-Nox2 mut reduces ROS production and vascular permeability by decreasing the TRPV4–Nox2 physical association.

Next, to verify this hypothesis, the following experiments were conducted. As shown in Fig. 5k–o, overexpressing Nox2 by tail-injection of AAV-Flt1-Nox2 into ND mice significantly increased its physical association with TRPV4 (Fig. 4b), the ROS production (Fig. 5k and Supplementary Fig. S7c), the permeability of primary aortic ECs (Fig. 5l, n), and decreased VE-cadherin and increased ICAM-1 mRNA expression (Fig. 5m). Therefore, AAV-Flt1-Nox2 increased the permeability of ND mouse aorta (Fig. 5o). Notably, overexpressing of Nox2 Δ4 into ND mice did not produce the same effects as that of

Nox2 (Fig. 5u–y and Supplementary Fig. S7d), which helped us establish the importance of the TRPV4–Nox2 physical association.

Furthermore, we also overexpressed Nox2 into TRPV4-KO mice (Fig. 5p–t). The results showed that overexpression of Nox2 had no effect on ROS production and vascular permeability in TRPV4-KO mice, confirming that enhancement of Nox2 expression increases ROS production and vascular permeability in a TRPV4 dependent manner.

Effect of chemical compound M12 in obesity-enhanced vascular permeability *via* regulation of the TRPV4–Nox2 physical association
The results shown in Fig. 5 indicate that altering the TRPV4–Nox2 physical interaction seems to be an effective way to regulate oxidative stress and vascular barrier disruption in obesity. Therefore, we set out to find a small molecule to disrupt the over-coupling of TPRV4 and Nox2 in obesity. Based on the three-dimensional structure of the TRPV4–Nox2 complex, we performed molecular docking analysis and screened a series of chemical compounds.

FRET assays in HEK cells co-expressing TRPV4 and Nox2 showed that gambogic acid, L755507, entrectinib, and M12 all significantly
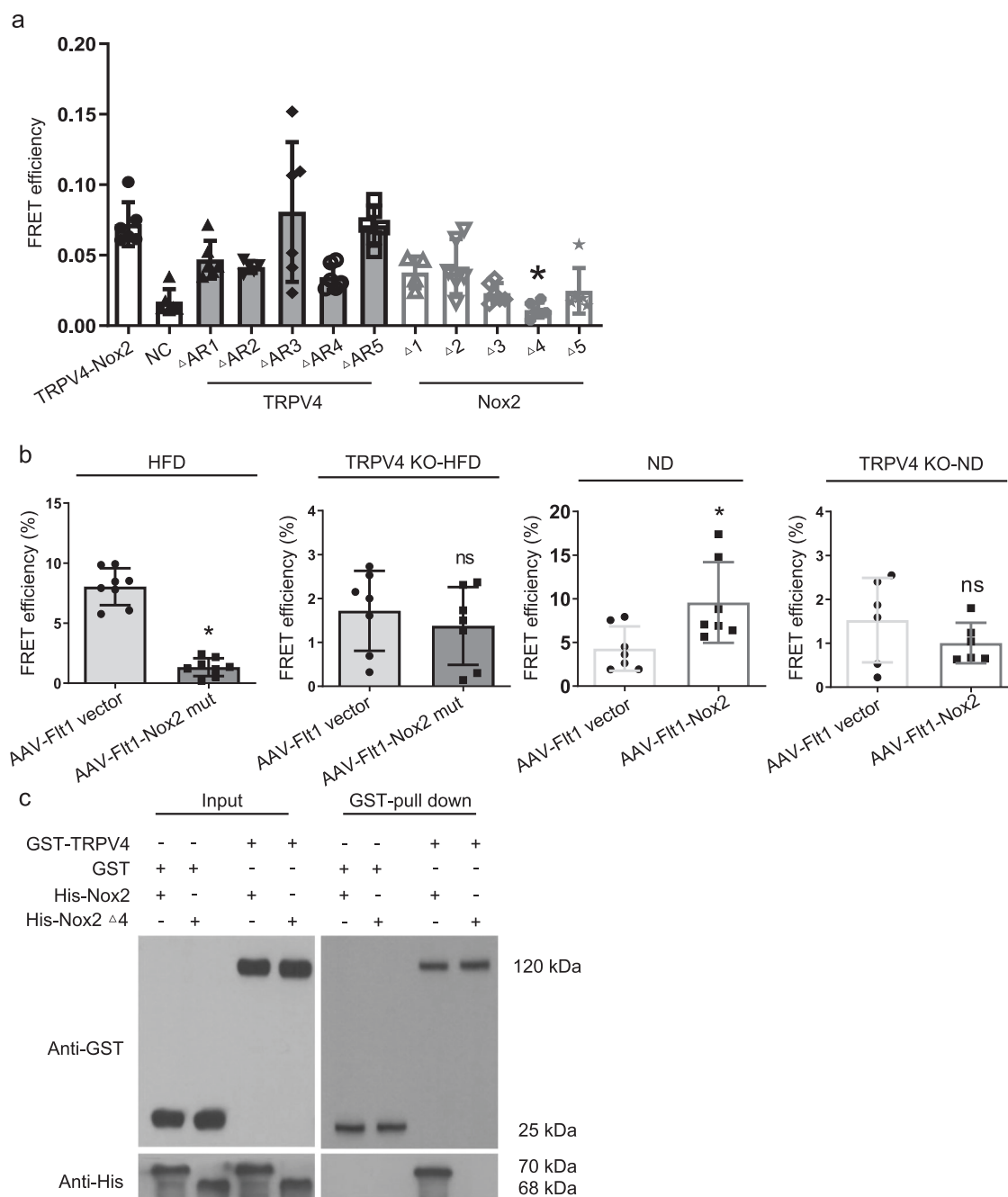
Fig. 4 Specific binding sites of TRPV4 and Nox2. a Statistics of FRET efficiency (TRPV4–Nox2 vs. Nox2-△4, $n = 4$–6 Petri dishes, $^*P = 0.0004$; one-way ANOVA, Dunnett's multiple comparisons test; otherwise, no significant difference; NC negative control). **b** FRET results in aorta ECs from ND, HFD, TRPV4 KO-ND, and TRPV4 KO-HFD mice pretreated with AAV-Flt1 vector, AAV-Flt1-Nox2, or AAV-Flt1-Nox2 mut (HFD, $n = 8$, $^*P < 0.0001$ vs. AAV-Flt1 vector; TRPV4-KO HFD, $n = 7$, $^*P = 0.4607$ vs. AAV-Flt1 vector; ND, $n = 7$, $^*P = 0.0379$ vs. AAV-Flt1 vector; TRPV4-KO, $n = 6$, $P = 0.2590$ vs. AAV-Flt1 vector. Student's t test, Mann–Whitney test for ND, otherwise, Student's t test, unpaired two-tailed t test). **c** GST pull-down assay showed that TRPV4 physically interacts with Nox2, the mutation of Nox2 destroys the interaction. All data are the mean ± SEM. △AR1-5 and △1-5, mutation at different binding sites of TRPV4 and Nox2; AAV-Flt1, endothelium-targeting adeno-associated virus.

decreased the FRET signal (Fig. 6a). Among these compounds, M12 (Fig. 6b and Supplementary Information 13) had the best effect. The optimal concentration of M12 was determined by MTT and Fret assay. The concentrations of M12 above 100 nM would result in cell death, while below 3 nM had no significant effect on the coupling of the TRPV4–Nox2 complex (Supplementary Fig. S9a, b). Besides, although M12 is an analogue of entrectinib, it is more effective in regulating TRPV4–Nox2 coupling and ROS production compared to entrectinib (Supplementary Fig. S9c–e).

Therefore, in the end, we chose 10 nM M12 for experiment. After determining the molecule and the dose to be used, we then determined whether M12 is a potent reducer of TRPV4–Nox2 coupling. We found that M12 disrupted the physical association between TRPV4 and Nox2 at 10 nM in obesity (Fig. 6c and Supplementary Fig. S10). CM-H₂DCFDA staining assays showed that M12 decreased ROS generation (Fig. 6d). Rhodamine phalloidin staining assays showed that M12 had a protective effect on cytoskeletal structure compared with HFD mouse aortic
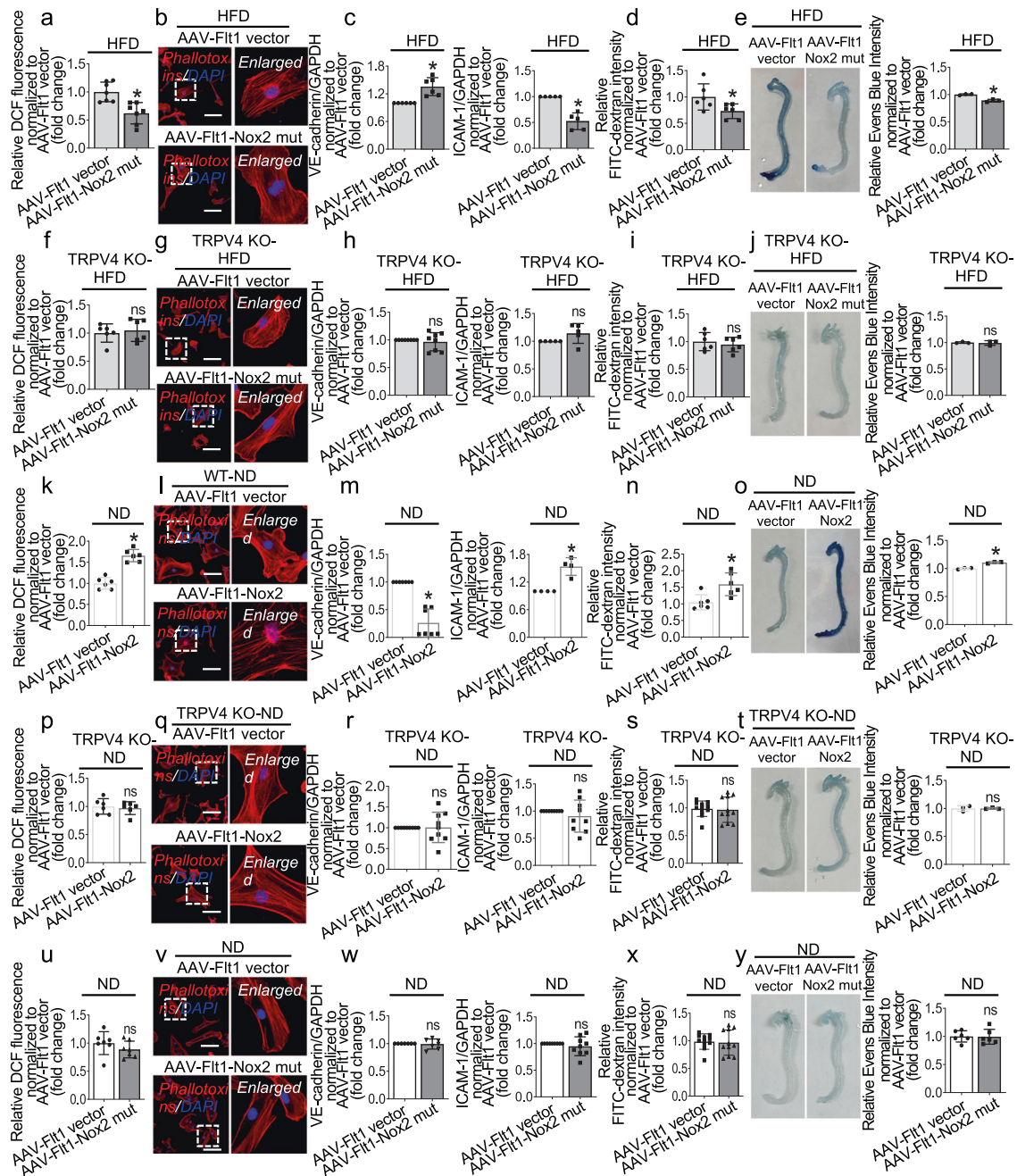
Fig. 5 Decreasing the TRPV4–Nox2 association lowers vascular permeability, while enhancing TRPV4–Nox2 association increases vascular permeability. a, f, k, p, u Quantification of relative DCF fluorescence in arterial segments isolated from HFD and TRPV4 KO-HFD mice after injection of AAV-Flt1 vector and AAV-Flt1-Nox2 mut (**a, f**) and from ND and TRPV4 KO-ND mice after injection of AAV-Flt1 vector, AAV-Flt1-Nox2 and AAV-Flt1-Nox2 mut (**k, p, u**). ($n = 6$–7 mice, $^{*}P < 0.05$ vs. AAV-Flt1 vector, Student's t test, unpaired two-tailed t test, otherwise, no significant difference). **b, g, l, q, v** Representative photomicrographs of rhodamine phalloidin staining in aortic ECs from HFD and TRPV4 KO-HFD mice after injection of AAV-Flt1 vector and AAV-Flt1-Nox2 mut (**b, g**) and from ND and TRPV4 KO-ND mice after injection of AAV-Flt1 vector, AAV-Flt1-Nox2 and AAV-Flt1-Nox2 mut (**l, q, v**). Scale bars, 100 μm. **c, h, m, r, w** Relative mRNA concentrations of VE-cadherin and ICAM-1 in aortic ECs as in (**a–u**) ($n = 4$–9 mice; $^{*}P < 0.05$ vs. AAV-Flt1 vector, Student's t test, paired t test, otherwise, no significant difference). **d, i, n, s, x** Relative intensity of FITC-dextran showing permeability of aortic ECs isolated from HFD and TRPV4 KO-HFD mice after injection of AAV-Flt1 vector and AAV-Flt1-Nox2 mut (**d, i**) and from ND and TRPV4 KO-ND mice after injection of AAV-Flt1 vector, AAV-Flt1-Nox2 and AAV-Flt1-Nox2 mut (**n, s, x**) ($n = 6$ mice; $^{*}P < 0.05$ vs. AAV-Flt1 vector, Student's t test, upaired t test, otherwise, no significant difference). **e, j, o, t, y** Relative content of Evans Blue per gram aorta from HFD and TRPV4 KO-HFD mice after injection of AAV-Flt1 vector and AAV-Flt1-Nox2 mut (**e, j**) and from ND and TRPV4 KO-ND mice after injection of AAV-Flt1 vector, AAV-Flt1-Nox2 and AAV-Flt1-Nox2 mut (**o, t, y**) ($n = 3$–6 mice; $^{*}P < 0.05$ vs. AAV-Flt1 vector, Student's t test, Paired t test, otherwise, no significant difference). All data are shown as the mean ± SEM. AAV-Flt1-Nox2 mut, Nox2 mutant AAV with a mutated region in the Nox2 and TRPV4 binding domain.
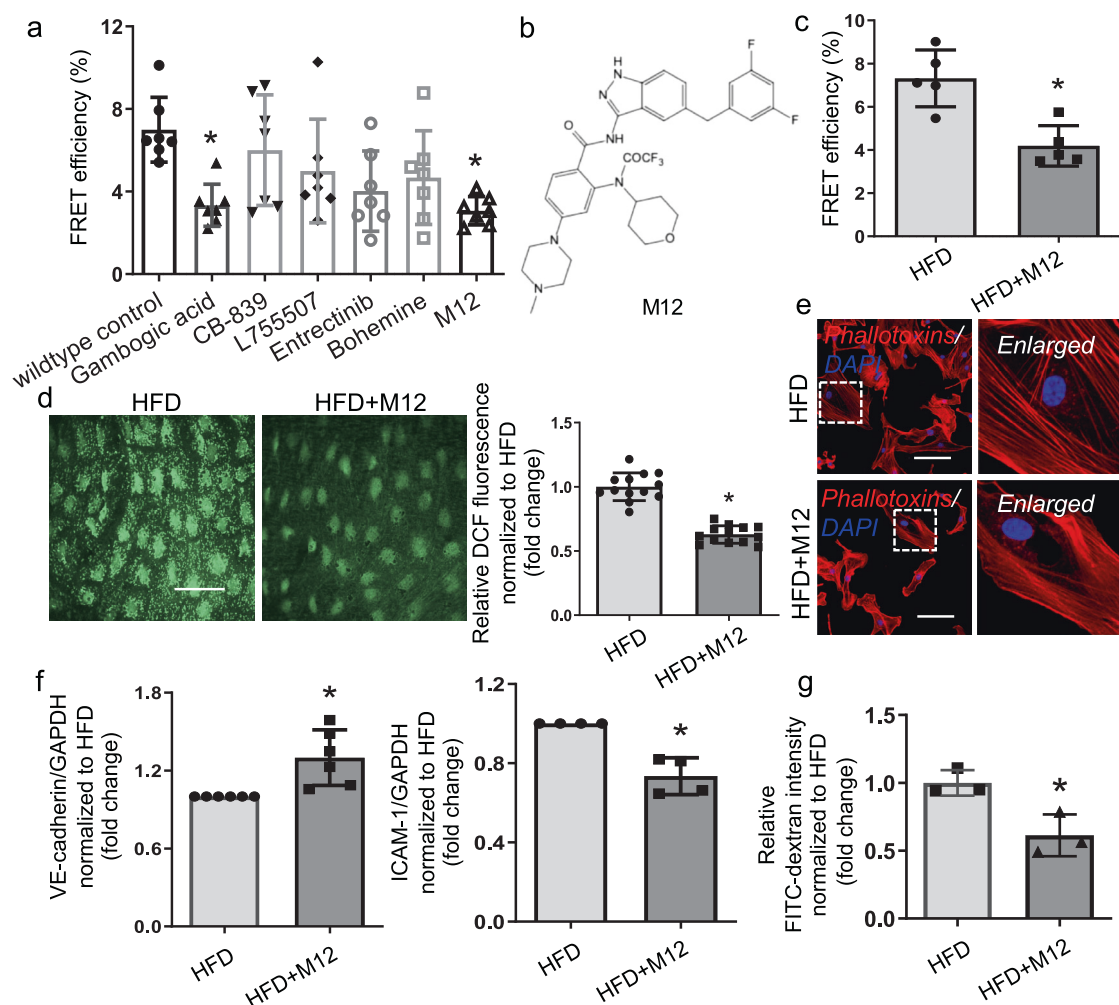
Fig. 6 Decreasing the TRPV4–Nox2 association with M12 improves obesity-induced vascular permeability. a Immuno-FRET results from HEK-293 cells transfected with Nox2 and TRPV4. Cells were pretreated with DMSO (0.1%), gambogic acid (1 μM), CB-839 (1 μM), L755507 (5 μM), entrectinib (10 nM), bohemine (1 μM), and M12 (10 nM) for 24 h ($n = 7$ Petri dishes; $^*P < 0.05$ vs. wild-type control TRPV4–Nox2, one-way ANOVA, Tukey's multiple comparisons test). **b** Structural formula of M12. **c** Immuno-FRET results in HFD aortic ECs pretreated with or without 10 nM M12 for 24 h ($n = 5$, $^*P = 0.0025$ vs. HFD, Student's t test, unpaired two-tailed t test). **d** Representative images and quantification of relative DCF fluorescence in arterial segments isolated from HFD mice pretreated with or without M12 (10 nM) for 24 h ($n = 13$, $^*P < 0.0001$ vs. HFD, Student's t test, unpaired two-tailed t test, scale bars, 50 μm). **e** Representative photomicrographs of rhodamine phalloidin staining in aortic ECs from HFD mice pretreated with or without M12 (10 nM) for 24 h (scale bars, 100 μm). **f** Relative mRNA concentrations of VE-cadherin and ICAM-1 in aortic ECs from HFD mice (VE-cadherin, $n = 6$ mice; $^*P = 0.0188$ vs. HFD; ICAM-1, $n = 4$; $^*P = 0.0107$ vs. HFD, Student's t test, Paired t test). **g** FITC-dextran staining assays showing the relative permeability of aortic ECs from HFD mice ($n = 3$) pretreated with M12 ($^*P = 0.0204$ vs. HFD, Student's t test, paired t test). All data are shown as the mean ± SEM.

ECs (Fig. 6e). Moreover, treatment with M12 also increased VE-cadherin and decreased ICAM-1 mRNA expression in obesity (Fig. 6f), decreased the degree of FITC-dextran extravasation (Fig. 6g), and improved excessive vascular permeability in the HFD mouse aorta. However, in the ND model, M12 had no influence (Supplementary Fig. S11). Further, we also performed experiments to examine whether M12 has an effect on the function and expression of TRPV4 or Nox2. The results of the immunoblotting assay showed that M12 does not affect the expression of TRPV4 or Nox2 (Supplementary Fig. S12a, b). Whole-cell patch clamp indicated that M12 treatment hardly has effect on GSK-induced whole-cell current (Supplementary Fig. S12c). CM-H$_2$DCFDA staining assay demonstrated that M12 treatment does not affect Nox2-induced ROS production Supplementary Fig. S12d). Together, these findings suggested that M12 alleviates oxidative stress and decreases vascular permeability by interrupting over-coupled endothelial TRPV4–Nox2 association in obesity, rather than affecting the function and expression of TRPV4 or Nox2.

DISCUSSION
Previous studies have focused on the function of TRPV4 or Nox2 alone [4, 8]. However, few studies have explored the function of TRPV4–Nox2 as a complex. In the present study, we used DIO mice as a tool and showed that the physical association between TRPV4 and Nox2 is significantly increased in DIO mice, and this was confirmed by co-IP and FRET assays. Then, with the GST pull-down assay, we provided, for the first time, evidence that TRPV4 interacts directly with Nox2 in vitro.

It is well known that the production of ROS is regulated by Nox2 [41, 42]. And now, as previous studies have shown, the production of ROS can also be regulated by TRPV4. Suresh et al. showed that TRPV4-mediated the inward flow of calcium affects ROS production, which is one of the causes of apoptosis during myocardial injury [43]. Other reports have suggested that TRPV4 is involved in the modulation of mitochondrial ROS production [7]. TRPV4 and Nox2 both play functional roles in regulating ROS generation. Also, our data showed that obesity-enhanced ROS generation and vascular

permeability can be attenuated by TRPV4 and Nox2 inhibitor, demonstrating the involvement of TRPV4 and Nox2 in regulating oxidative stress and abnormal vascular permeability in obesity. However, the involvement of the TRPV4–Nox2 interaction in this regulation has seldom been reported. In this study, one of the most important findings was that TRPV4–Nox2 interaction is involved in regulating ROS generation and vascular permeability. Then, using AAV, we demonstrated that interrupting the physical association between TRPV4 and Nox2 can help reduce oxidative stress and abnormal vascular permeability in obesity. We also provided evidence that TRPV4 functionally associates with Nox2. In this way, our results, in addition to supporting the findings of previous studies [7, 43, 44], also provide a new mechanism that can explain the vascular barrier disruption in obese mice. Because TRPV4 and Nox2 are widely expressed and are involved in regulating important physiological functions [45–48], their systemic activation by drugs often has serious side-effects. Based on these issues, it is urgent and important to explore additional therapeutic modalities. Here, we showed that TRPV4–Nox2 may be a potential therapeutic target for excessive oxidative stress and vascular barrier disruption. Using DS studio, another principal finding was that M12 significantly decreased the excessive physical association between TRPV4 and Nox2 in obesity without impairing their function and expression. More importantly, M12 reversed the vascular barrier disruption through modulating the TRPV4–Nox2 interaction.

However, the present study is subject to limitations. First, we focused on the action of M12 on the TRPV4–Nox2 complex, while the effects of M12 on other members of the NADPH oxidase family remain to be further investigated. Second, although we found that M12 regulated permeability, due to time constraints, we only validated this effect at the cellular level, but not through an in-depth study in mice. Third, although we have confirmed that TRPV4 physically and functionally associates with Nox2, it is unclear whether this functional codependence had to occur through a physical interaction. These issues are to be investigated in our follow-up.

In conclusion, our study suggests for the first time that TRPV4 physically and functionally associates with Nox2. The TRPV4–Nox2 complex is essential to modulate obesity-induced abnormal vascular permeability. Obesity enhances the physical association between TRPV4 and Nox2, which increases the generation of ROS. Excessive oxidative stress disrupts cytoskeletal structure, alters the levels of VE-cadherin and ICAM-1 expression, and finally impairs vascular permeability. In this study, we provided novel evidence to reveal the potential of TRPV4–Nox2 as an anti-oxidative stress therapeutic target for abnormal vascular permeability and identified a compound, M12, capable of targeting this complex, providing a new concept for the development of new drugs with fewer side-effects.

AUTHOR CONTRIBUTIONS
MRG and XM designed the research; JH, PZ, HK, XPH, and HJL performed the research; CLT contributed new reagents or analytic tools; MRG and YFZ analyzed the data and wrote the paper.

ADDITIONAL INFORMATION
Supplementary information The online version contains supplementary material available at https://doi.org/10.1038/s41401-021-00780-8.

Competing interests: XM, CLT, MRG, and JH have applied to the State Intellectual Property Office of China for the patent "A compound for reducing TRPV4–Nox2 excessive interaction and its application in anti-abnormal vascular permeability" (2020114600923).

REFERENCES
1. Mundi S, Massaro M, Scoditti E, Carluccio MA, van Hinsbergh VWM, Iruela-Arispe ML, et al. Endothelial permeability, LDL deposition, and cardiovascular risk factors. Cardiovasc Res. 2018;114:35–52.
2. Ohara Y, Peterson TE, Harrison DG. Hypercholesterolemia increases endothelial superoxide anion production. J Clin Invest. 1993;91:2546–51.
3. Xu L, Nagata N, Ota T. Glucoraphanin: a broccoli sprout extract that ameliorates obesity-induced inflammation and insulin resistance. Adipocyte. 2018;7:218–25.
4. Filosa JA, Yao X, Rath G. TRPV4 and the regulation of vascular tone. J Cardiovasc Pharmacol. 2013;61:113–9.
5. Wu QF, Qian C, Zhao N, Dong Q, Li J, Wang BB, et al. Activation of transient receptor potential vanilloid 4 involves in hypoxia/reoxygenation injury in cardiomyocytes. Cell Death Dis. 2017;8:e2828.
6. Hamanaka K, Jian MY, Townsley MI, King JA, Liedtke W, Weber DS, et al. TRPV4 channels augment macrophage activation and ventilator-induced lung injury. Am J Physiol Lung Cell Mol Physiol. 2010;299:L353–62.
7. Bubolz AH, Mendoza SA, Zheng X, Zinkevich NS, Li R, Gutterman DD, et al. Activation of endothelial TRPV4 channels mediates flow-induced dilation in human coronary arterioles: role of Ca^{2+} entry and mitochondrial ROS signaling. Am J Physiol Heart Circ Physiol. 2012;302:H634–42.
8. Burgoyne JR, Mongue-Din H, Eaton P, Shah AM. Redox signaling in cardiac physiology and pathology. Circ Res. 2012;111:1091–106.
9. Song Q, Zhang Y. Application of high-fat cell model in steady-state regulation of vascular function. Saudi J Biol Sci. 2019;26:2132–5.
10. Gao M, Han J, Zhu Y, Tang C, Liu L, Xiao W, et al. Blocking endothelial TRPV4-Nox2 interaction helps reduce ROS production and inflammation, and improves vascular function in obese mice. J Mol Cell Cardiol. 2021;157:66–76.
11. Suzuki M, Mizuno A, Kodaira K, Imai M. Impaired pressure sensation in mice lacking TRPV4. J Biol Chem. 2003;278:22664–8.
12. Meoli L, Isensee J, Zazzu V, Nabzdyk CS, Soewarto D, Witt H, et al. Sex- and age-dependent effects of Gpr30 genetic deletion on the metabolic and cardiovascular profiles of diet-induced obese mice. Gene. 2014;540:210–6.
13. Ma X, Du J, Zhang P, Deng J, Liu J, Lam FF, et al. Functional role of TRPV4-KCa2.3 signaling in vascular endothelial cells in normal and streptozotocin-induced diabetic rats. Hypertension. 2013;62:134–9.
14. Adebiyi A, Zhao G, Narayanan D, Thomas-Gatewood CM, Bannister JP, Jaggar JH. Isoform-selective physical coupling of TRPC3 channels to IP3 receptors in smooth muscle cells regulates arterial contractility. Circ Res. 2010;106:1603–12.
15. Kropf DL, Berge SK, Quatrano RS. Actin localization during fucus embryogenesis. Plant Cell. 1989;1:191–200.
16. Lee DH, Park JS, Lee YS, Han J, Lee DK, Kwon SW, et al. SQSTM1/p62 activates NFE2L2/NRF2 via ULK1-mediated autophagic KEAP1 degradation and protects mouse liver from lipotoxicity. Autophagy. 2020;16:1949–73.
17. Cao C, Edwards A, Sendeski M, Lee-Kwon W, Cui L, Cai CY, et al. Intrinsic nitric oxide and superoxide production regulates descending vasa recta contraction. Am J Physiol Ren Physiol. 2010;299:F1056–64.
18. Shao J, Han J, Zhu Y, Mao A, Wang Z, Zhang K, et al. Curcumin induces endothelium-dependent relaxation by activating endothelial TRPV4 channels. J Cardiovasc Transl Res. 2019;12:600–7.
19. Salazar G, Cullen A, Huang J, Zhao Y, Serino A, Hilenski L, et al. SQSTM1/p62 and PPARGC1A/PGC-1alpha at the interface of autophagy and vascular senescence. Autophagy. 2020;16:1092–110.
20. Choi N, Kim WS, Oh SH, Sung JH. Epiregulin promotes hair growth via EGFR-medicated epidermal and ErbB4-mediated dermal stimulation. Cell Prolif. 2020;53:e12881.
21. Thengchaisri N, Hein TW, Ren Y, Kuo L. Endothelin-1 impairs coronary arteriolar dilation: Role of p38 kinase-mediated superoxide production from NADPH oxidase. J Mol Cell Cardiol. 2015;86:75–84.
22. Zhou Z, Rajamani U, Labazi H, Tilley SL, Ledent C, Teng B, et al. Involvement of NADPH oxidase in A2A adenosine receptor-mediated increase in coronary flow in isolated mouse hearts. Purinergic Signal. 2015;11:263–73.
23. El-Awady MS, Rajamani U, Teng B, Tilley SL, Mustafa SJ. Evidence for the involvement of NADPH oxidase in adenosine receptors-mediated control of coronary flow using A1 and A3 knockout mice. Physiol Rep. 2013;1:e00070.
24. Chen S, Jiang H, Wu X, Fang J. Therapeutic effects of quercetin on inflammation, obesity, and type 2 diabetes. Mediators Inflamm. 2016;2016:9340637.
25. Vieira AA, Michels M, Florentino D, Nascimento DZ, Rezin GT, Leffa DD, et al. Obesity promotes oxidative stress and exacerbates sepsis-induced brain damage. Curr Neurovasc Res. 2015;12:147–54.

26. Timmerman I, Heemskerk N, Kroon J, Schaefer A, van Rijssel J, Hoogenboezem M, et al. A local VE-cadherin and Trio-based signaling complex stabilizes endothelial junctions through Rac1. J Cell Sci. 2015;128:3514.

27. Barry AK, Wang N, Leckband DE. Local VE-cadherin mechanotransduction triggers long-ranged remodeling of endothelial monolayers. J Cell Sci. 2015;128:1341–51.

28. Barry AK, Tabdili H, Muhamed I, Wu J, Shashikanth N, Gomez GA, et al. Alpha-catenin cytomechanics-role in cadherin-dependent adhesion and mechanotransduction. J Cell Sci. 2014;127:1779–91.

29. Giannotta M, Trani M, Dejana E. VE-cadherin and endothelial adherens junctions: active guardians of vascular integrity. Dev Cell. 2013;26:441–54.

30. Yan M, Zhang X, Chen A, Gu W, Liu J, Ren X, et al. Endothelial cell SHP-2 negatively regulates neutrophil adhesion and promotes transmigration by enhancing ICAM-1-VE-cadherin interaction. FASEB J. 2017;31:4759–69.

31. Domazetovic V, Bonanomi AG, Stio M, Vincenzini MT, Iantomasi T. Resveratrol decreases TNFalpha-induced ICAM-1 expression and release by Sirt-1-independent mechanism in intestinal myofibroblasts. Exp Cell Res. 2019;382:111479.

32. Bodiga VL, Kudle MR, Bodiga S. Silencing of PKC-alpha, TRPC1 or NF-kappaB expression attenuates cisplatin-induced ICAM-1 expression and endothelial dysfunction. Biochem Pharmacol. 2015;98:78–91.

33. Bodiga VL, Inapurapu SP, Vemuri PK, Kudle MR, Bodiga S. Intracellular zinc status influences cisplatin-induced endothelial permeability through modulation of PKCalpha, NF-kappaB and ICAM-1 expression. Eur J Pharmacol. 2016;791:355–68.

34. Vitoria WO, Thome LS, Kanashiro-Galo L, Carvalho LV, Penny R, Santos WLC, et al. Upregulation of intercellular adhesion molecule-1 and vascular cell adhesion molecule-1 in renal tissue in severe dengue in humans: Effects on endothelial activation/dysfunction. Rev Soc Bras Med Trop. 2019;52:e20180353.

35. Kim Y, Lee S, Zhang H, Lee S, Kim H, Kim Y, et al. CLEC14A deficiency exacerbates neuronal loss by increasing blood-brain barrier permeability and inflammation. J Neuroinflammation. 2020;17:48.

36. Shi Y, Xiong Y, Lei Y, Li Z, Yan H, Yuan J, et al. Protective effect of COMP-angiopoietin-1 on peritoneal vascular permeability and peritoneal transport function in uremic peritoneal dialysis rats. Am J Transl Res. 2019;11:5932–43.

37. Chen H, Tong X, Lang L, Jacobson O, Yung BC, Yang X, et al. Quantification of tumor vascular permeability and blood volume by positron emission tomography. Theranostics. 2017;7:2363–76.

38. Zhao H, Zhu Y, Zhang J, Wu Y, Xiang X, Zhang Z, et al. The beneficial effect of hes on vascular permeability and its relationship with endothelial glycocalyx and intercellular junction after hemorrhagic shock. Front Pharmacol. 2020;11:597.

39. Jeong J, Lee J, Lim J, Cho S, An S, Lee M, et al. Soluble RAGE attenuates AngII-induced endothelial hyperpermeability by disrupting HMGB1-mediated crosstalk between AT1R and RAGE. Exp Mol Med. 2019;51:1–15.

40. Lundeberg E, Van Der Does AM, Kenne E, Soehnlein O, Lindbom L. Assessing large-vessel endothelial permeability using near-infrared fluorescence imaging. Arterioscler Thromb Vasc Biol. 2015;35:783–6.

41. Suresh K, Servinsky L, Jiang H, Bigham Z, Yun X, Kliment C, et al. Reactive oxygen species induced Ca^{2+} influx via TRPV4 and microvascular endothelial dysfunction in the SU5416/hypoxia model of pulmonary arterial hypertension. Am J Physiol Lung Cell Mol Physiol. 2018;314:L893–907.

42. Lyons JS, Joca HC, Law RA, Williams KM, Kerr JP, Shi G, et al. Microtubules tune mechanotransduction through NOX2 and TRPV4 to decrease sclerostin abundance in osteocytes. Sci Signal. 2017;10:506.

43. Wu Q, Lu K, Zhao Z, Wang B, Liu H, Zhang S, et al. Blockade of transient receptor potential vanilloid 4 enhances antioxidation after myocardial ischemia/reperfusion. Oxid Med Cell Longev. 2019;2019:7283683.

44. Hong Z, Tian Y, Yuan Y, Qi M, Li Y, Du Y, et al. Enhanced oxidative stress is responsible for TRPV4-induced neurotoxicity. Front Cell Neurosci. 2016;10:232.

45. Suresh K, Servinsky L, Reyes J, Baksh S, Undem C, Caterina M, et al. Hydrogen peroxide-induced calcium influx in lung microvascular endothelial cells involves TRPV4. Am J Physiol Lung Cell Mol Physiol. 2015;309:L1467–77.

46. Naziroglu M, Oz A, Yildizhan K. Selenium and neurological diseases: focus on peripheral pain and TRP channels. Curr Neuropharmacol. 2020;18:501–17.

47. Martner A, Aydin E, Hellstrand K. NOX2 in autoimmunity, tumor growth and metastasis. J Pathol. 2019;247:151–4.

48. Kroller Schon S, Daiber A, Steven S, Oelze M, Frenis K, Kalinovic S, et al. Crucial role for Nox2 and sleep deprivation in aircraft noise-induced vascular and cerebral oxidative stress, inflammation, and gene regulation. Eur Heart J. 2018;39:3528–39.